Magnetic and optical anisotropy of *Clostridium pasteurianum* rubredoxin from optically detected electron paramagnetic resonance

Birgit Börger and Dieter Suter
Fachbereich Physik, Universität Dortmund, 44221 Dortmund, Germany

(Received 27 April 2001; accepted 14 September 2001)

The high-spin Fe(III)-center of oxidized rubredoxin from *Clostridium pasteurianum* shows a complicated, temperature-dependent EPR spectrum. We combine conventional EPR spectroscopy with optically detected EPR (ODEPR) to elucidate the electronic structure of this protein metal center. The ODEPR experiment, which can be considered as coherent Raman scattering or modulated magnetic circular dichroism (MCD), yields spectra that depend on the relative orientation of optical and magnetic dipole moments. A detailed analysis of the spectra shows that they correspond to a zero-field splitting of $D=+46.3\,\mathrm{GHz}$ and a strong rhombic distortion with $E/D=0.25$. In the frozen solution, conformational strain gives rise to variation of the rhombicity, which can be measured quantitatively from the EPR line shape. Analysis of the ODEPR line shapes yields the orientation of the optical anisotropy with respect to the magnetic *g*-tensor. We compare the results from this study to published results on EPR, optical spectroscopy, and MCD. © *2001 American Institute of Physics.* [DOI: 10.1063/1.1415461]

I. INTRODUCTION

Rubredoxins are small proteins containing a single $[\mathrm{Fe(S\text{-}Cys)_4}]$-cluster, which are involved in electron transfer processes. A detailed understanding of their electronic structure has been a major goal of many spectroscopic studies. Electron paramagnetic resonance[1,2] revealed the approximately rhombic symmetry of the ground state. In contrast, optical techniques, such as single crystal polarized absorption spectroscopy[3] and magnetic circular dichroism (MCD) spectroscopy[4–7] indicated a nearly axial site symmetry, leading to an interpretation of the optical spectra in terms of an effective D_{2d} symmetry.

Here we report the first detailed analysis of the rather complicated EPR spectrum of rubredoxin in frozen solution. The lowest energy doublet has a very strong anisotropy, resulting in a relatively nonspecific, broad EPR line. The higher doublets become populated and contribute to the spectrum only at increasing temperatures. These signals allow us to quantify the zero-field splitting, including its sign and rhombicity. The medium energy doublet shows a characteristic EPR line shape that can be quantitatively interpreted in terms of variations of the crystal field, i.e., conformational strain.

To get additional information about the orientation of the *g*-tensor axes, we use a recently developed optically detected EPR technique.[8] As in the conventional experiment, a resonant microwave field excites transverse magnetization, which is detected by a circularly polarized laser beam propagating perpendicular to the static magnetic field. The precessing spins modulate the circular dichroism of the sample and thereby the amplitude of the laser beam at the microwave frequency. Measuring this modulation as a function of magnetic field strength yields ODEPR spectra, where different components of the optical anisotropy contribute to different parts of the spectrum. A detailed analysis of these spectra allows us to extract the relative orientation of the optical dipoles relative to the axes of the spin Hamiltonian. The present work is the first application of this technique to a high spin system.

II. ELECTRON PARAMAGNETIC RESONANCE

A. Spin Hamiltonian

An adequate spin Hamiltonian describing the ground-state of a Fe(III)-high spin complex ($S=5/2$) is

$$\mathcal{H}=\mu_B g(B_x\hat{S}_x+B_y\hat{S}_y+B_z\hat{S}_z) + D(\hat{S}_z^2-1/3S(S+1))+E(\hat{S}_x^2-\hat{S}_y^2), \quad (1)$$

where μ_B is the Bohr magneton, g is the isotropic g-value ($g=2$), and the B_i are the components of the static magnetic field along the corresponding crystal field axis. D and E are the second rank axial and rhombic coefficients, respectively, of the zero-field spin Hamiltonian. It is convention in EPR spectroscopy to choose the axes of the spin Hamiltonian such that $E/D\leqslant 1/3$. For an axial case system E vanishes, whereas in an extreme rhombic geometry it becomes $E=D/3$. For rubredoxin, a slight deviation from extreme rhombic symmetry is observed.[1]

The eigenvalues of the Hamiltonian (1) depend strongly on the direction of the external magnetic field with respect to the principal axes of the zero-field Hamiltonian. Figure 1 represents these energies as a function of the field strength for the cases where the field is oriented along one of the three principal axes. For small fields, the states can be described as three Kramers doublets, which are well separated by the zero-field splitting of approximately $(4\sqrt{7}/3)D\simeq 3.5D$. These doublets can be treated as effective spins $S=1/2$, and effective g-values can be determined for each doublet. For positive D and $E/D=0.25$, the effective g-values are summarized in Table I.[1]

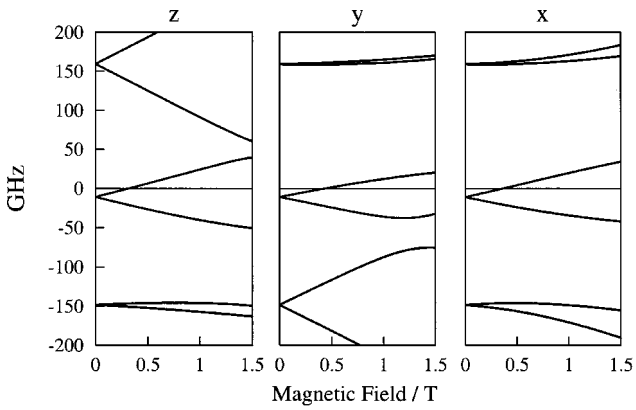

FIG. 1. Energy levels as a function of magnetic field applied along the three principal directions of rubredoxin for zero field splitting parameters $D=46.3$ GHz and $E/D=0.25$.

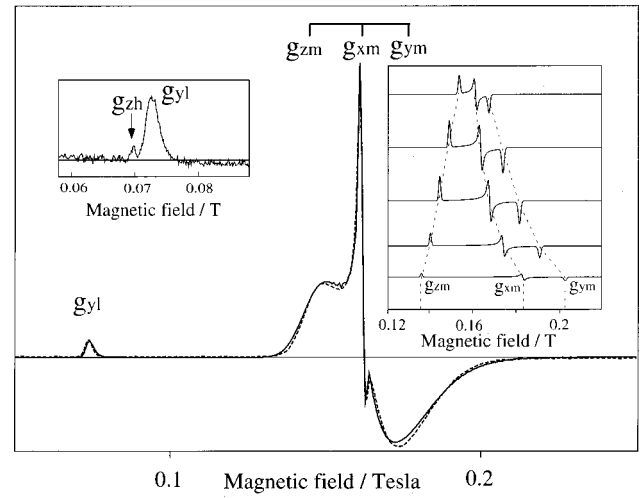

FIG. 2. Conventional EPR spectrum (derivative of absorption) of rubredoxin, at $T=8.1$ K, $\nu=9.6$ GHz (dashed line) and fit curve (solid line). Right hand inset: several calculated EPR spectra with different ratios E/D, centered at $E/D=0.25$. Left hand inset: Detail of the EPR spectrum measured at $T=18$ K.

Although it is normally the convention in EPR to label the largest g-value g_z and the smallest g_x, we use here the axis system defined by the zero-field spin Hamiltonian for all Kramers doublets.

For negative values of D, the g-values for highest and lowest doublet would be interchanged. The nonlinear variation of the energies at high fields, evident from the figure, indicates that the analysis of the system in terms of three independent doublets starts to break down at fields $B>1$T.

B. Conventional EPR spectra

Recombinant rubredoxin of *Clostridium pasteurianum* expressed in *E. coli* was purchased from Sigma. The experiments were performed on a buffered, aequeous solution of rubredoxin, where the buffer was TRIS with a *p*H of 7.4. The solution was mixed with a glassing agent (glycerol 1:1), resulting in a concentration of 0.5 mM. For the conventional EPR measurements a Bruker ER200D SRC X-band spectrometer with a rectangular TE_{102} cavity operating at 9.6 GHz was used.

We measured conventional EPR spectra of *Clostridium pasteurianum* rubredoxin at three different temperatures: 4 K, 8.1 K, and 18.8 K. The spectrum at 8.1 K is depicted in Fig. 2. The dominating feature between 0.12 and 0.2 T, corresponding to g-values in the range 3.4–5.7 stems from the medium energy doublet, while the peak at 0.07 T is due to $g_{yl}=9.4$. The inset on the left shows how this spectral region changes when the temperature is raised to $T=18$ K. The additional feature on the low-field side, corresponding to $g=9.84$, must be attributed to an excited doublet. As the energy level scheme in Fig. 1 and the discussion in the previous section show, it can only be attributed to $g_{zh}=9.84$. This assignment of g-values is compatible with a rhombicity $E/D=0.25$ and a positive zero-field splitting D; for $D<0$, the largest g-value would be in the ground state doublet. This result agrees with data from *Pseudomonas oleovorans*.[2]

To determine the absolute value of the zero-field splitting, we fitted the EPR spectra quantitatively as a function of temperature. We used a numerical diagonalization of the full ($S=5/2$) spin Hamiltonian for a given E and D to calculate effective principal g-values for the three doublets. For each of the Kramers doublet, we then calculated a powder spectrum according to well-established methods.[9] The resonance condition is in this case[10] $\hbar\omega_0=g_{\mathrm{eff}}(\theta,\phi)\mu_B B_0$, where

$$g_{\mathrm{eff}}^2(\theta,\phi)=g_{z_{\mathrm{eff}}}^2\cos^2\theta+(g_{x_{\mathrm{eff}}}^2\cos^2\phi+g_{y_{\mathrm{eff}}}^2\sin^2\phi)\sin^2\theta. \quad (2)$$

The angles θ and ϕ define the orientation of the static magnetic field B_0 in the molecular (g-tensor) coordinate system. The result of such a fit is depicted in Fig. 2 for a spectrum measured at 8.1 K. The zero-field splitting can be determined from the relative size of the ground state signal ($g_{yl}=9.4$) versus the medium energy region of the spectrum. The results from the three spectra are well compatible with each other, yielding a zero-field splitting of $D=46.3\pm2.1$ GHz. This agrees with results from by Mössbauer studies ($D=57.8\pm8$ GHz, Ref. 11) within the experimental errors as well as with previous EPR studies from *Pseudomonas oleovorans* rubredoxin, where $D=52.8$ GHz was obtained.[1]

The splitting in the spectrum of the medium energy doublet is a direct measure of the deviation from complete rhombicity. While the positions of the three resonances are well compatible with a ratio $E/D=0.25$, the overall shape differs from the usual powder spectra. In particular, the low- and high-field resonances are significantly broader than the center peak. This pattern cannot originate from g-strain, i.e., a statistical distribution of the g-values, since this would result in equal broadening of all three resonances. A-strain can also

TABLE I. Effective g-values for rubredoxin ($D=46.3$, $E/D=0.25$).

Kramers doublet	Effective g-values
lowest	$g_{zl}=0.92$, $g_{yl}=9.4$, $g_{xl}=1.45$
medium	$g_{zm}=4.76$, $g_{ym}=3.76$, $g_{xm}=4.08$
highest	$g_{zh}=9.84$, $g_{yh}=0.36$, $g_{xh}=0.47$

be ruled out, since the nuclear spin of the most abundant Fe-isotope, ^{56}Fe, is zero. On the other hand, we find excellent agreement between the experimental data and spectra calculated for a statistical variation of E/D. A distribution of E/D indicates conformational strain and has been observed for other high-spin ferric proteins.[12,13] A representative set of spectra calculated for different values of E/D is depicted in the right hand inset of Fig. 2. In analogy to the more familiar case of "g-strain," we refer to this effect as "E/D"-, or rhombicity-strain. The best agreement between theoretical and experimental spectra was obtained for a Gaussian distribution of E/D values around a center value of 0.25 and a width of $\sigma_{E/D}=0.03$. The same ratio was used at all three temperatures.

III. OPTICALLY DETECTED EPR

A. Fundamentals

An alternative to the conventional detection of EPR is the optical detection by coherent Raman scattering.[14] The optical detection allows one to deduce the relative orientation of the g-tensor with respect to the optical dipole tensor.[15,16,8] For an (effective) spin $S=1/2$ ground state with three distinct g-values and a powderlike sample, the microwave modulated, transverse MCD $\Delta\epsilon_x$ along the direction of laser beam propagation is[16]

$$\Delta\epsilon_x \propto \int_{\theta=0}^{\pi/2}\int_{\phi=0}^{\pi/2} T(\theta,\phi) f(\sigma)\left[C_z g_z \frac{g_\perp^2}{g^2}\sin^2\theta + C_x\left(\frac{g_x^3 g_z^2}{g^2 g_\perp^2}\cos^2\theta\cos^2\phi + \frac{g_x g_y^2}{g_\perp^2}\sin^2\phi\right) + C_y\left(\frac{g_y^3 g_z^2}{g^2 g_\perp^2}\cos^2\theta\sin^2\phi + \frac{g_y g_x^2}{g_\perp^2}\cos^2\phi\right)\right] \times \sin\theta\, d\theta\, d\phi, \quad (3)$$

where $T(\theta,\phi)=\tanh(g(\theta,\phi)\mu_B B_0/2kT)$ is the Boltzmann factor, $g_\perp^2=g_x^2\cos^2\phi+g_y^2\sin^2\phi$, and $f(\sigma)$ is a line shape function with linewidth σ. The three parameters C_i, $i=x, y, z$ describe the optical anisotropy along the three principal axes, which are assumed to coincide with the principal axes of the g-tensor. These anisotropy parameters may be expressed by the optical dipole operators m_j and m_k:[15]

$$C_i=\epsilon_{ijk}\,\mathrm{Im}\sum_E \langle G|m_j|E\rangle\langle E|m_k|G\rangle. \quad (4)$$

The sum runs over the excited states $|E\rangle$, $|G\rangle$ are the relevant ground states, and ϵ_{ijk} represents the antisymmetric Levi–Civita tensor.

Since the optical anisotropy depends on the orientation of the molecule with respect to the laser beam, the ODEPR detection sensitivity is also orientation dependent. Figure 3 summarizes this effect: the three spectra represent the situation where the optical anisotropy is oriented along a specific molecular axis, while the orthogonal directions show no MCD effect. If the C_i term dominates, the spectral region around g_i is strongly attenuated compared to the conventional EPR spectrum shown at the bottom of the figure.

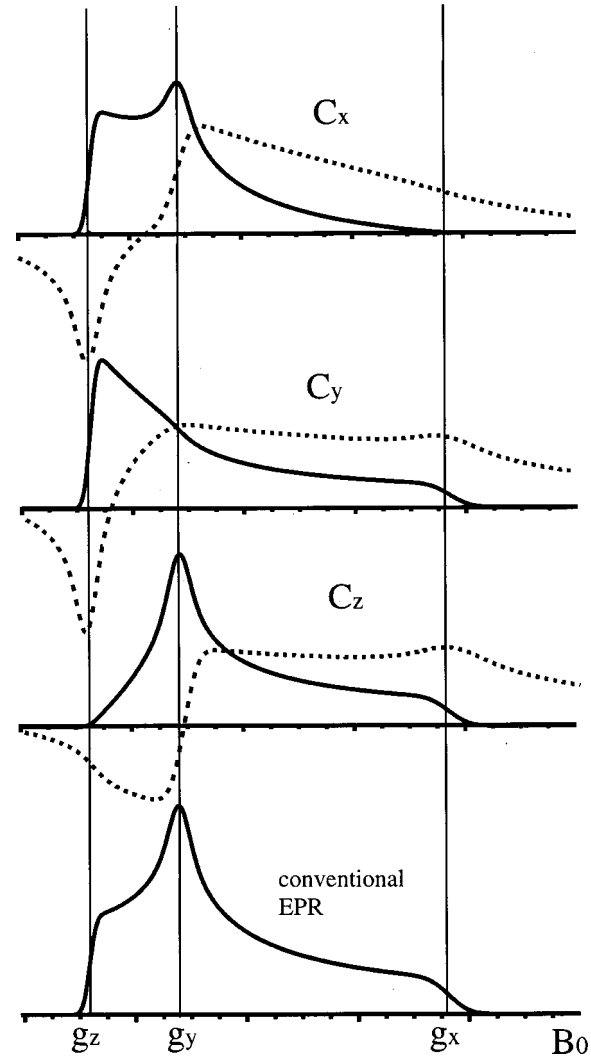

FIG. 3. Calculated ODEPR absorption and dispersion spectra for different optical anisotropies of a $S=1/2$ molecule with three distinct g-values. The first three traces correspond to optical detection when only a single molecular axis shows optical anisotropy. The bottom trace corresponds to the conventional EPR spectrum for the same parameters.

B. Experimental results

The rubredoxin sample was prepared in the same way as for the EPR experiment with a concentration of approximately 0.14 mM. The optical pathlength was 0.5 mm. Fast quenching of the solution in liquid helium yielded a glass with good optical quality. The sample was placed in a rectangular cavity and excited by a weak microwave field with a frequency of 13.7 GHz. A variable magnetic field was provided by a superconducting split coil magnet. The laser beam propagated through the sample at a right angle to the static magnetic field and parallel to the microwave field, to detect the precessing magnetization. We used three different laser sources to cover the wavelength range from 450 to 560 nm, where the charge transfer transitions are expected: an argon-ion laser for the wavelengths between 459 and 514 nm, a diode-pumped, frequency doubled Nd:YVO_4 laser with a single line at 532 nm, and a ring dye-laser with Rhodamine 110 between 545 and 560 nm. The amplitude modulation of the transmitted light was detected with a high-speed photo-

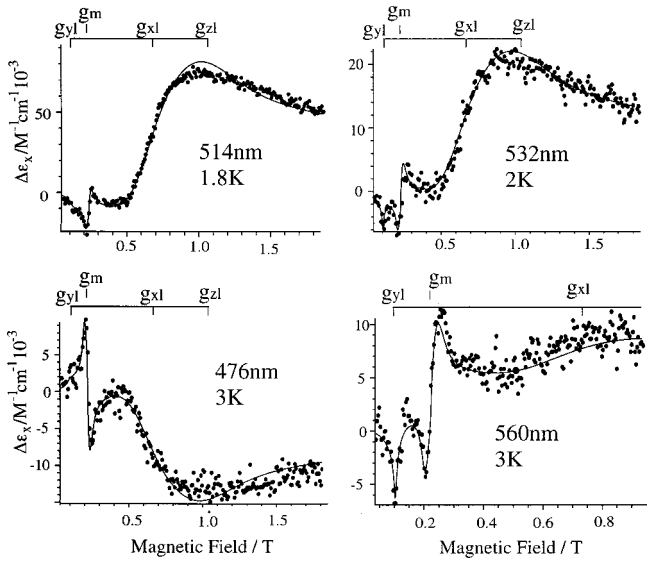

FIG. 4. Four experimental ODEPR spectra measured at different wavelengths (points) in units of $\Delta\epsilon_x \times 10^{-3}\,\mathrm{M}^{-1}\,\mathrm{cm}^{-1}$. The solid lines represent the fitted spectra at the given temperatures.

diode (bandwidth 21 GHz, diameter of active area 25 μm). Demodulation of this microwave signal with a quadrature mixer allowed the simultaneous detection of absorption and dispersion components of the EPR signal. The polarization of the light was modulated between right and left circularly polarized by a photoelastic modulator. A more detailed discussion of the instrument has been published elsewhere.[17]

Figure 4 gives a survey of the strong variation of the ODEPR line shape with the wavelength of the detection laser. The figure contains four spectra measured at different wavelengths at a temperature of 1.8 K and microwave frequency of 13.7 GHz, as indicated by dots. The microwave power was 120 mW for the spectra at 514 and 560 nm, and 180 mW for the spectra at 476 and 532 nm.

The spectra are plotted as $\Delta\epsilon_x$, the difference in extinction coefficients for left and right circularly polarized light. Only the dispersion signal is given, since the absorption signal is strongly saturated under our experimental conditions. Characteristic for the dispersion line shape are the very strong high field tails.

At 1.8 K the spectra are dominated by the low energy Zeeman doublet. The medium energy doublet contributes only via a rather small feature around $B=0.25$ T where different g-values are not well resolved for the dispersion. As a consequence, the spectrum at 514 nm is dominated by the g_{xl}-resonance around 0.7 T. No resonance from g_{yl}, which is expected at 0.1 T can be seen. The spectrum at 476 nm exhibits similar features, except that the sign of the spectrum is reversed and the medium doublet resonance is larger.

At 532 nm (right hand column, upper trace of Fig. 4), the spectrum is comparable to the 514 nm spectrum, but includes an additional resonance at 0.1 T. The 560 nm spectrum is dominated by the low field features (0.1 and 0.2 T).

C. Wavelength-dependence of optical anisotropy

To show how the relative orientation of optical and magnetic anisotropy affects the MCD-detected EPR spectrum,

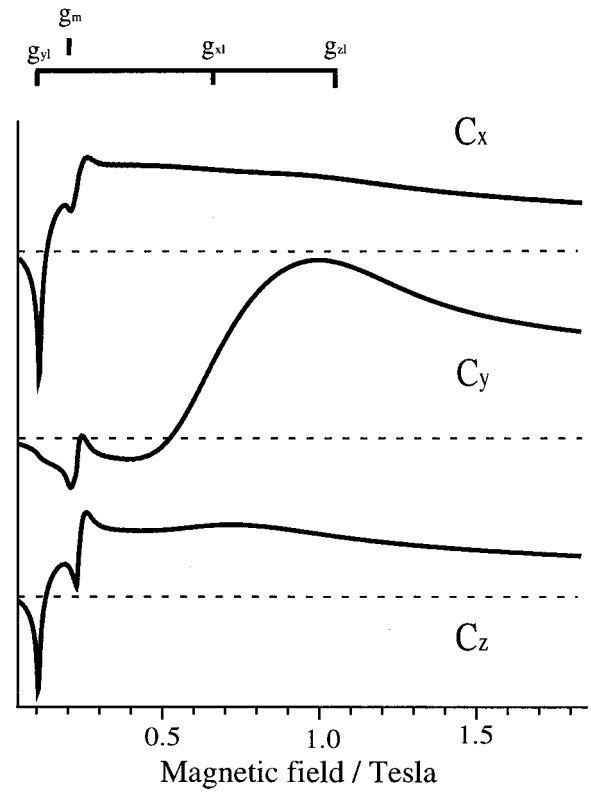

FIG. 5. Three calculated dispersion type ODEPR spectra calculated with the parameters of the conventional EPR ($D=46.3$, $E/D=0.25$, $\sigma_{E/D}=0.03$). The upper trace shows a spectrum expected for exclusively C_x-polarization, the middle trace C_y-polarization, and the bottom trace C_z-polarization. The g-values of the lowest and the medium energy doublet are also given. The temperature was set as 1.8 K.

Fig. 5 shows three prototypical rubredoxin ODEPR dispersion spectra, calculated with the parameters from the conventional EPR spectra. They represent the three extreme cases of exclusively C_x-polarization ($C_y=C_z=0$), C_y-polarization ($C_x=C_z=0$), and C_z-polarization ($C_x=C_y=0$). The temperature was set to 1.8 K, the resonance frequency was 13.7 GHz. The first and the third curve, which show low intensity in the high field region, look rather similar. This effect stems from the small difference between g_{xl} and g_{zl} in comparison to g_{yl}, resulting in a quasi-axial arrangement. In addition, the E/D-strain obscures the high field features. The second curve is due to C_y only, which means that the $g_{yl}=9.4$ resonance is strongly suppressed and $g_{xl}=1.45$ dominates the spectrum. The medium energy doublet, indicated by g_m, contributes only via a small dispersionlike peak at 0.25 T.

To determine the optical anisotropy at different wavelengths, we fitted each spectrum, keeping the EPR parameters obtained from the conventional spectra and adjusting the C_α. The ODEPR spectrum measured at 514 nm, shown in Fig. 4, is very similar to the second trace in Fig. 5, indicating that the main signal contribution is due to C_y. Fitting the experimental spectrum indicated 92% C_y-polarization; the fitted spectrum is shown as a solid line in Fig. 4.

The agreement between the theoretical and experimental spectrum is remarkably good in the low field range and quite satisfactory above 0.5 T, which is dominated by $g_{xl}=1.45$. Although at a field higher than 1 T the concept of effective

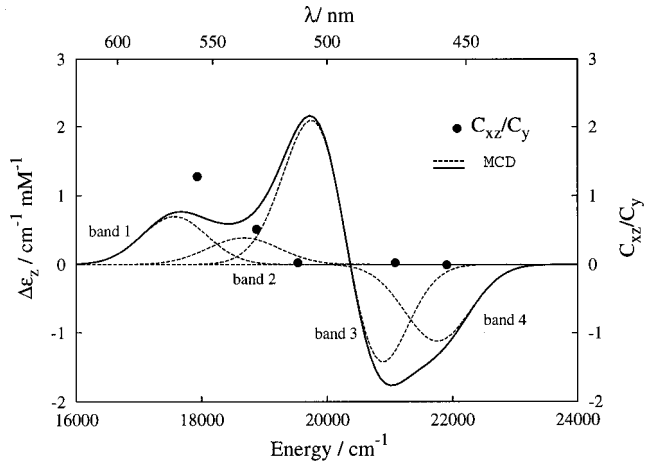

FIG. 6. Four low energy charge-transfer bands of the MCD spectrum of rubredoxin (according to Ref. 6). The solid curve is the total (longitudinal) MCD resulting from these bands. The ratio of C_{xz}/C_y from ODEPR is also given in the figure (right hand scale).

g-values is not strictly valid any more, we found that the ODEPR dispersion line shape is relatively insensitive to the exact position of the high-field g_{zl}-value. Thus the $S=1/2$ approach is still a good approximation and allows us to characterize the optical transition at 514 nm as polarized along the crystal field *x*- and *z*-axis.

The sign reversal from 514 to 476 nm parallels the sign reversal in the MCD spectrum (Fig. 6). At 476 nm the $g_m=4.3$ resonance is somewhat larger than in the 514 nm spectrum; this is probably due to a slight heating of the sample by the laser beam caused by higher intensity. We found that a local temperature of 3 K gave good results for the fit, while a temperature of 1.8 K did not produce a satisfactory fit of the $g_m=4.3$ resonance. The temperature increase by 1.2 K leads to a significantly higher population of the medium doublet. Experimental and theoretical spectra are superimposed in Fig. 4, and the local temperature extracted from the fit is indicated for each spectrum. The optical anisotropy was again found to be predominantly C_y. Similar results were obtained at 458 nm (not shown), where a local temperature of 2.2 K gave optimal results.

While the spectra at short wavelengths are dominated by the C_y anisotropy, we find significant contributions from C_x and C_z at longer wavelengths. Fits show that the contribution of C_x and C_z are practically undistinguishable. This agrees with the approximately axial symmetry found in the optical spectra.[3] We therefore used axial symmetry for the optical system, using $C_{xz}=1/2(C_x+C_z)$. Within this model, we found that the ratio C_{xz}/C_y is approximately 0.5 at 532 nm. Toward longer wavelengths the $g=9$ peak becomes increasingly prominent, as shown in the spectrum measured at 560 nm, which has very little intensity in the high field region. This reveals a strong dipole along the molecular *y*-axis. From the fit we determined the ratio of C_{xz}/C_y as approximately 1.3.

We restricted our experiments to the low temperature region where the spectrum is dominated by the low energy doublet. Since the magnetic anisotropy is extremely large for this doublet, it is feasible to make conclusions about optical anisotropy even with a relatively poor signal-to-noise ratio. Inspection of the experimental spectra shows that the medium doublet is not sufficiently resolved to allow a detailed analysis of the line shape.

TABLE II. Relevant parameters for the four low energy charge transfer bands. The optical polarization as determined from ODEPR is given in the last column.

Band number	Band number acc. to Ref. 6	Center energy (Ref. 6)	MCD pattern (Ref. 6)	Polarization from ODEPR
1	1	17 541	Gaussian	$C_{xz}/C_y=1.4\pm0.4$
2	6	18 975	Gaussian	$C_{xz}/C_y=1.0\pm0.4$
3	4	20 243	Gauss. deriv.	$C_{xz}/C_y=0\pm0.1$
4	5	21 739	Gaussian	$C_{xz}/C_y=0\pm0.1$

D. Relation to MCD

ODEPR can be considered as microwave-modulated MCD.[18,8] Correspondingly, the optical properties derived from these experiments are closely related to longitudinal MCD spectra. The MCD of *desulfovibrio gigas* rubredoxin was analyzed in detail by Oganesyan *et al.*[6] to derive the electronic structure of the Fe center. They were able to identify six charge transfer transitions in the visible and near UV region of the spectrum. Four of these transitions fall into the spectral range covered by our experiments; the relevant data for these transitions are summarized in Table II.

In Fig. 6 we show these four low energy charge transfer bands.[6] Bands 1, 2, and 4 have a Gaussian line shape, while band 3 is correlated with a group theoretical *E*-term and appears therefore as an asymmetrical Gaussian derivative shape. Also given in this figure is the ratio C_{xz}/C_y as determined from ODEPR measurements measured at the corresponding wavelengths (right hand scale, filled circles). The ratio C_{xz}/C_y is close to zero for band 3 and band 4, indicating dominant C_y polarization. At 560 nm (17 857 cm^{-1}) the ratio C_{xz}/C_y is 1.3, indicating that band 1 has a significant C_{xz}-contribution and thus a dipole along the crystal field *y*-axis. The considerable C_{xz}-polarization at 532 nm (18 797 cm^{-1}) agrees well with the weak band 2 situated at this position which also has a strong dipole along *y*. Following our earlier procedure,[8] we determined the polarization of band 1 as $C_{xz}/C_y=1.4$ and band 2 to be approximately $C_{xz}/C_y=1.0$. These assignments are summarized in Table II.

These findings can be compared with the assignment of the rubredoxin optical bands made on the basis of D_{2d}-symmetry.[3,5,6] The spectral features in the visible have been assigned to charge-transfer transitions $S\rightarrow$Fe(III). Oxidized rubredoxin has a ground state $^6A_1$. A transition $^6A_1\rightarrow{}^6B$ must have significant polarization along the D_{2d}-symmetry axis, and on the basis of single crystal polarization data this was assigned to band 1 at 17 541 cm^{-1}. In contrast, a transition from $^6A_1$ to the ^6E-state is polarized in a plane perpendicular to the D_{2d}-symmetry axis, and this has been assigned to the derivative-shaped band 3 at 18 975 cm^{-1} and the band 4 at 21 739 cm^{-1}. Band 2 has been assigned to arise from a weak distortion from D_{2d}-symmetry and to show a strong dipole along the optical symmetry axis.

Within the D_{2d} analysis of the rubredoxin, the ODEPR analysis unambiguously shows that the direction of the largest g-value (the crystal field y-axis in standard EPR notation) coincides with the S_4-axis. This finding is in agreement with Ref. 5 and 6. Our assignment can be readily verified by considering band 3, for which single crystal polarized absorption spectroscopy[3] showed that it is polarized in the plane perpendicular to the D_{2d}-symmetry axis, while our experimental data are only compatible with C_y optical anisotropy. Thus the spin Hamiltonian y axis must be parallel to the symmetry axis.

IV. GENERAL CONCLUSIONS

The electronic structure of the high spin Fe^{3+}-ion in rubredoxin has been debated extensively. Optical and EPR studies have provided most of the relevant parameters, but a number of details, such as the orientation of the interaction tensors, the sign and size of the zero-field splitting have remained elusive. We have applied coherent Raman detected EPR spectroscopy to *Clostridium pasteurianum* rubredoxin, in combination with conventional EPR spectroscopy. We found a positive sign of the zero-field Hamiltonian (in the usual EPR notation), with the numerical values $D=+46.3\,\mathrm{GHz}$ and $E=+11.6\,\mathrm{GHz}$, which refines the predicted values from Mössbauer studies.[11] The ratio $E/D=0.25$ corresponds to a small but highly significant deviation from a fully rhombic system. In addition, an analysis of the line shape gave clear indication of "E/D-strain," indicating that the protein is present in a number of similar conformations. Similar results have been reported for other systems on the basis of high resolution laser spectroscopy.[19–21]

The orientation of the g-tensor could be identified by optically detected EPR: the EPR spectra correlate the optical anisotropy tensor with the g-tensor, clearly indicating that the optical symmetry axis is parallel to the direction of the largest g-value (the y-axis in the usual EPR notation). The analysis of the ODEPR spectra also gave improved values for the optical polarization of the charge transfer transitions in the 400–600 nm wavelength region. This work represents the first application of this technique to a high-spin system and an Fe–S protein; extensions to similar systems should be straightforward.

ACKNOWLEDGMENTS

The authors thank Dr. Vasily Oganesyan for helpful discussions, and Dr. Stephen J. Bingham and Jörg Gutschank for experimental assistance. Support by the DFG through the Graduiertenkolleg Festkörperspektroskopie and Project No. SU 192/9-1 is gratefully acknowledged.

[1] J. Peisach, W. E. Blumberg, E. T. Lode, and M. J. Coon, J. Biol. Chem. **246**, 5877 (1971).
[2] W. E. Blumberg and J. Peisach, Ann. N.Y. Acad. Sci. **222**, 539 (1973).
[3] W. Eaton and W. A. Lovenberg, "The iron-sulfur complex in rubredoxin," in *Iron-Sulfur Proteins* (Academic, New York, 1973).
[4] J. C. Rivoal, B. Briat, R. Cammack, D. O. Hall, K. K. Rao, I. N. Douglas, and A. J. Thomson, Biochim. Biophys. Acta **493**, 122 (1977).
[5] D. E. Bennett and M. K. Johnson, Biochim. Biophys. Acta **911**, 71 (1986).
[6] V. S. Oganesyan, S. J. George, M. R. Cheesman, and A. J. Thomson, J. Chem. Phys. **110**, 762 (1999).
[7] V. S. Oganesyan and A. J. Thomson, J. Chem. Phys. **113**, 5003 (2000).
[8] B. Börger, S. J. Bingham, J. Gutschank, D. Suter, and A. J. Thomson, J. Am. Chem. Soc. **123**, 2334 (2001).
[9] J. R. Pilbrow, *Transition Ion Electron Paramagnetic Resonance* (Oxford University Press, Oxford, 1990).
[10] A. Abragam and B. Bleaney, *Electron Paramagnetic Resonance of Transition Ions* (Oxford University Press, Oxford, 1961), Chap. 3.
[11] C. Schulz and P. G. Debrunner, J. Phys. Colloq. **37**, 153 (1976).
[12] A. S. Yang and B. J. Gaffney, J. Biophys. Soc. **51**, 55 (1987).
[13] B. J. Gaffney and H. J. Silverstone, J. Magn. Res. **134**, 57 (1998).
[14] S. J. Bingham, D. Suter, A. Schweiger, and A. J. Thomson, Chem. Phys. Lett. **266**, 543 (1997).
[15] S. J. Bingham, B. Börger, J. Gutschank, D. Suter, and A. J. Thomson, JBIC **5**, 30 (2000).
[16] S. J. Bingham, J. Gutschank, B. Börger, D. Suter, and A. J. Thomson, J. Chem. Phys. **113**, 4331 (2000).
[17] S. J. Bingham, B. Börger, D. Suter, and A. J. Thomson, Rev. Sci. Instrum. **69**, 3403 (1998).
[18] B. Börger, S. J. Bingham, J. Gutschank, D. Suter, and A. J. Thomson, J. Chem. Phys. **111**, 8565 (1999).
[19] J. Schlichter, J. Friedrich, L. Herenyi, and J. Fidy, J. Chem. Phys. **112**, 3045 (2000).
[20] H. Frauenfelder, S. G. Sligar, and P. G. Wolynes, Science **254**, 1598 (1991).
[21] W. Köhler, J. Friedrich, and H. Scheer, Phys. Rev. A **37**, 660 (1988).